DEM and soil bin study on a biomimetic disc furrow opener

Yueming Wang[a], Weiliang Xue[b], Yunhai Ma[a], Jin Tong[a], Xianping Liu[c], Jiyu Sun[a,]

[a] *Key Laboratory of Bionic Engineering (Ministry of Education), Jilin University, Changchun, 130022, P. R. China*

[b] *YTo Group Corporation, Luoyang, 471039, P. R. China*

[c] *School of Engineering, University of Warwick, Coventry CV4 7AL, UK*

Abstract

To reduce the resistance and energy consumption of disc furrow openers, biomimetic coupling disc furrow openers (BCDFOs) that were inspired by digging animals (e.g., the convex hull of a dung beetle pronotum and the back-ridge scales of a pangolin) were designed as biomimetic coupling elements. The resistance of BCDFOs, analyzed by the discrete element method, was less than that of the common flat disc furrow opener (CFDFO). The effects of different structures on soil disturbances in the forward and lateral directions were analyzed. The soil swelling rate and soil disturbance coefficient were calculated to evaluate the soil disturbance characteristics. Three less resistant BCDFOs were manufactured and tested in soil bins with different working conditions (furrow speed = 0.6, 1 and 1.4 m/s; soil moisture contents = 18% and 22%). It was found that the furrow resistance of the BCDFOs was obviously less than that of the CFDFO under the same test conditions, thus indicating that the BCDFO concept was an efficient bioinspired design for efficient agriculture tillage.

Key words: biomimetic; disc furrow opener; resistance reduction; DEM; soil disturbance.

1. Introduction

No-tillage systems have been developed since the late 20th century to realize the sustainable and stable production of agricultural resources, protecting land resources

Corresponding author: sjy@jlu.edu.cn
Tel:+86-0431-85095760
Fax: +86-0431-85095760ext888

from soil erosion in the black soil zone of Northeast China. The furrow opener is the key working part of no-tillage seeders. Traditional openers often stick to soil during furrow operations, which changes the working trajectory and increases the traction resistance. The seeding furrows often fail to meet seed requirements, which reduces crop emergence rates. Operating a traditional agricultural tillage system (e.g., furrow opener and tillage blade) uses 30%-50% of its total energy to overcome sliding resistance between the soil and tillage surface due to soil adhesion and friction (Zhang et al., 2016).

In furrowing with a double disc furrow opener, the furrow resistance is mainly generated by its interaction with soil. Specifically, the disc cuts soil while crushing, lifting and turning the cut soil, so the furrowing resistance is influenced by three processes: disk cutting soil, soil movement, and soil-disc slip (Ahamad and Amran, 2004). There are several types of openers that are adaptive to varying crop demands and soil types. The main furrow openers include the double-end pointed shovel type, shoe type, pointed bar type, and runner/sword type, which are feasible for light-to-modest soil, black soil, heavy soil, and shallow sowing, respectively (Mkomwa et al., 2015). The energy required to pull a tool through soil is a function of tool geometry and soil conditions (Chi and Kushwaha, 1990). Resistance due to soil adhesion can be reduced by various methods (Sakane and Maeyama, 1993), such as surface-modified material (Salokhe and Gee-Clough, 1987, 1988, 1989, Jia, 2006), lubrication (Tong et al., 1999), electro-osmosis (Ren et al., 2001, Spagnoli et al., 2011) and vibration (Wang et al., 1998). New opener structures with inverted “T” shapes (Chaudhary, 1988, Khan et al., 1990), arc cutting edge shapes (Gou et al., 2012), duckbill shapes (Zhao et al., 2013) or mole shapes (Deng et al., 1986) have been explored in combination with soil and climate conditions to meet the special seeding requirements in different planting areas. The groove created by an inverted-T-shaped opener is narrow at the top and wide at the bottom. Despite the large tillage resistance, field tests show that new openers noticeably accelerate seed emergence compared with traditional openers. No-tillage seeding openers with arc cutting edge shapes have high passing ability, with a high corn stubble cutting rate of 86%. The limited soil

disturbance is applicable to no-tillage wheat seeding in the hilly areas of Southwest China. The duckbill shaped opener with a duckbill-like head and a sword-like tip is suitable for soil cutting. The entire head buries in soil with high penetrability, and it is not easily jammed by grasses during ditching. The overall structure of the mole shaped opener is approximately columnar with a soil cutting edge at the front. In operation, the entire opener buries into the soil and raises the soil in situ. The mole shaped opener, a simple structure, is able to robustly prepare the soil, but it is unsuitable for heavy clay soils. Moreover, seeds and fertilizers cannot be simultaneously applied.

Animals living in moist soil develop special geometric features that are advantageous to reduce soil adhesion after years of evolution. They have the most efficient digging action with the lowest energy consumption in soil, and they rarely or never experience soil adhesion to ensure free movement (Tong et al., 2009). The seeder opener always adheres to soil during the interaction with soil, which increases energy consumption and damages of the ditch shape to slow crop emergence. Therefore, it is practically significant to simulate the surficial structures of animals adapted to living in soil, and design biomimetic ditching parts based on them with reduced drag properties.

During the furrowing process, the disc cutting edge of a double disc opener first cuts soil and then pushes the soil away from its surface to form a groove (Ahmadi, 2017). In this process, its surface is squeezed and rubbed by soil. Similar to the ditching of a disc, dung beetles and pangolins use their pronotum and back scales, respectively, to squeeze and push away soil, forming a passage or cave upon moving. After long-term natural selection, the pronotum of the dung beetle and the back scales of the pangolin have formed excellent body surface structures to adapt to movement in soil. The nonsmooth body surface structures effectively reduce the soil adhesion area and limit water film continuity, improving the interfacial lubrication against soil resistance (Ren, 2009a).

In this study, the microconvex structure of the dung beetle head and the protruding structure of the pangolin back scales were used as biomimetic coupling

elements to design biomimetic coupling disc furrow openers (BCDFOs). Then, resistance simulation was carried out by the discrete element method (DEM), and the optimal BCDFO and a common flat disc furrow opener (CFDFO) were compared in soil bin tests.

2. Materials and Methods

2.1 Design of BCDFOs

BCDFOs were designed by adding a biomimetic coupling structure onto the surfaces of CFDFOs. The microconvex structure of the dung beetle head and the protruding structure of the pangolin back scales are shown in Fig. 1. First, 3D models of CFDFOs were established in SolidWorks 2014. The whole structure of CFDFOs was generated with the extrude command with hollow cylinders, and the cutting edge of the furrow disc was generated using the scan-cut command. According to the working characteristics of no-tillage disc furrow openers in Northeast China, a commercial CFDFO was chosen with a diameter = 300 mm, a thickness = 3 mm, an intersection angle of double discs = 11.5°, and a rake angle = 10.21°.

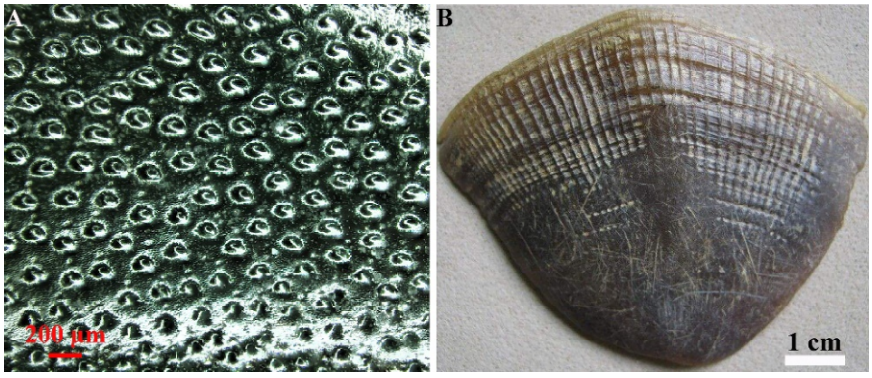

Fig. 1. Two types of biomimetic structural elements.

The biomimetic coupling elements were regularly or irregularly arranged on the matrix. The machining accuracy of irregular arrangements was uncontrollable and high-cost, so regular arrangements were selected. The two coupling elements were alternatively arranged in a ring on the disc surfaces.

The appropriate arrangement of biomimetic coupling elements on the disc was an important controlling factor on the biomimetic effect. If the number of arranged elements was too small, the most soil contacted the disc and the limited convexity hindered the soil movement, which increased the furrowing resistance. If the number

of arranged elements was too large, the moisture tension was almost unchanged, and the water film at the contact interface was more likely to be continuous, which was unfavorable for reducing resistance (Jia, 2006).

Biomimetic coupling elements were arranged circularly around the disc center, and the rest of their characteristics could be generated by the circle array method. The arrangement of biomimetic coupling elements on the furrow disc is shown in Fig. 2, with the following structural parameters: biomimetic coupling element angle with a ring θ=7.2, 9 and 12°; element spacing between different rings S_1= 2, 4 and 6 mm; distance from the outmost biomimetic unit to the disc edge S_2=5 mm; layer number of ring coupling element n=3; and wedge height h_2=3 mm, wedge weight d=6 mm, and wedge length L= dimension of convex hull D. There were four factors, each with three levels.

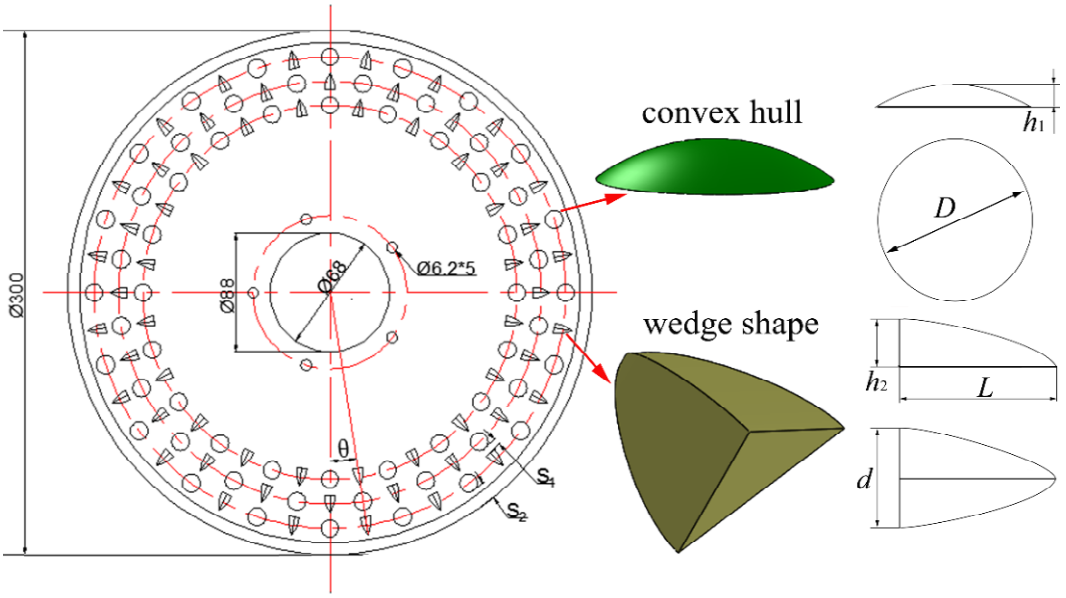

Fig. 2. Structural parameters of the BCDFO design

An orthogonal experimental optimization design, which reduced the number of tests and controlled the test variables, was used to simplify the analysis (Ren, 2009b). In this paper, the furrow resistance in the horizontal direction F was used as the test index, and the independent variables D, h_1, S_1 and θ were used to design the orthogonal experiment. The test factor level of disc furrow resistance is shown in Table 1.

Table 1. Test factor level of disc furrow resistance

level \ factor	h_1 (mm)	D (mm)	S_1 (mm)	θ (°)
1	1	6	2	12
2	3	10	4	9
3	4	14	6	7.2

BCDFOs composed of biomimetic coupling elements of multiple sizes in different arrangements were studied to optimize the scheme of low-adhesion and low-resistance biomimetic opener discs. These BCDFOs provided a reference for designing low-energy and low-adhesion furrow opener discs. According to L(3^4) by the optimization design method, 9 kinds of BCDFO models were built, numbered DISC 1 to 9. The common flat disc furrow opener (CFDFO) was numbered DISC 10 (as shown in Fig. 3).

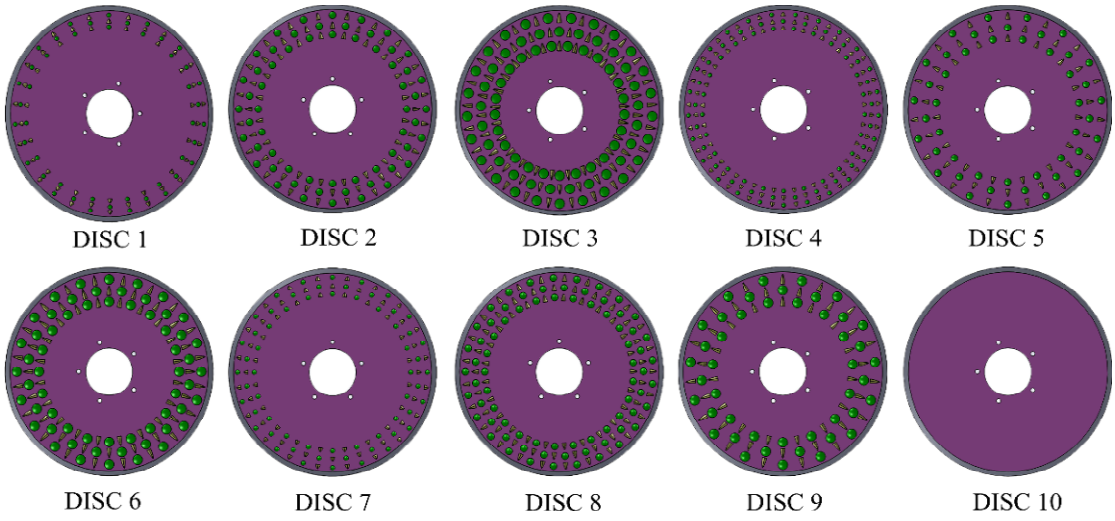

Fig. 3. BCDFO models (DISC 1-9) and CFDFO model (DISC 10).

2.2 DEM simulation

The interaction between the furrow opener disc and soil was simulated by DEM, which is a useful tool to examine the dynamic behavior of granular media and optimize the disc design (Ucgul et al., 2014). As soil is a complex inhomogeneous material, the reliability of simulation results was decided by the selection of the constitutive relation. The Hertz-Mindlin contact model was chosen for the DEM simulation. In Northeast China, the tillage soil is primarily sticky black soil that easily agglomerates. Based on the soil cutting of an opener disc and the entire furrow time,

the soil model was created with 1500 (length) ×400 (width) ×430 (height) mm^3 dimensions.

The setting of parameters was closely related to the soil adhesion. Stacking angle test was used to calibrate discrete element parameters of soil. The geometric model of virtual test of stacking angle was established in EDEM software according to the measurement method of soil stacking angle to obtain the stacking angle regression model by multivariate regression fitting analysis of test results (Barr et al., 2018). The optimized parameters could be used to simulate the sample soil with discrete element between the clay soil and the contact soil parts. In this paper, according to the relevant references (Barr et al., 2018, Ucgul et al., 2014, Barr and Fielke, 2016, Asaf et al., 2007, Das, 2008, Budynas and Nisbett, 2012), some experiments have shown that these parameters were consistent with the characteristics of northeast black soils, as shown in Table 2.

The setting of soil particle size also had a significant effect on the simulation results and simulation time. If the particle size was too small, the simulation calculation time would be greatly increased, and if too big, it would be affect the authenticity of the simulation. In order to balance the calculation time and the authenticity of the simulation results, the particle size was usually scaled up. According to the relevant references, the radius of 4-6 mm can meet the performance requirements of simulation calculation and make the simulation results without obvious distortion (Barr et al., 2018). In this paper, the soil particles were randomly generated in a soil bin with a radius of 4-6 mm.

Table 2 Main material properties used in the DEM simulation

Property	Value
Density of soil particles (kg/m^3)	1350
Density of steel (kg/m^3)	7865
Poisson's ratio of soil	0.3
Poisson's ratio of steel	0.3
Shear modulus of steel (MPa)	7.9×10^4

Shear modulus of soil (MPa)	1×10^6
Coefficient of static friction of soil-soil	0.5
Coefficient of static friction of soil-steel	0.5
Coefficient of rolling friction of soil-soil	0.3
Coefficient of rolling friction of soil-steel	0.4
Coefficient of restitution of soil-soil	0.2
Number of soil elements	516000

2.3 Testing parameters in the soil bin

The soil bin test was carried out from July to September 2016 at the College of Biological and Agricultural Engineering, Jilin University. The soil bin was 30 m (length) × 3 m (width) × 0.8 m (height) and filled with black soil. The soil was treated by rotary tillage, repression and water spray to meet the requirements of the soil moisture and firmness of 262.5 in 50 mm for testing. The actual furrow speed was approximately 0.5-2 m/s. Therefore, three speeds of 0.6 1.0 and 1.4 m/s were tested in the soil bin with the test vehicle operating smoothly. The moisture content was important to the disc resistance (Ren, 2009b). The suitable moisture content for seeds was approximately 20%. In this paper, the resistance of the disc was tested at soil moistures of 18% and 22%. The furrow depth was set at 70 mm.

3. Results and Discussion

3.1 DEM simulation

Taking DISC 10 as an example, the interaction between the disc and the soil proceeded through four main stages: A, the opener just contacting the soil; B, the opener fully immersing in the soil; C, the opener just leaving the soil; and D, the opener fully out of the soil (Fig. 4). The furrow resistance increased gradually from A to B and then fluctuated along a constant value from B to C. When the disc just left the soil, the furrow resistance increased suddenly, which was due to the broken soil (Ahmadi, 2017). When the disc left the soil, the microcrack in front of the disc did not exist, which would increase the furrow resistance. From C to D, the furrow resistance decreased gradually. The average value of the stable fluctuation stage from B to C was used as the furrow resistance. Generally, a smaller furrow resistance represented

a better performance, which meant less energy consumption.

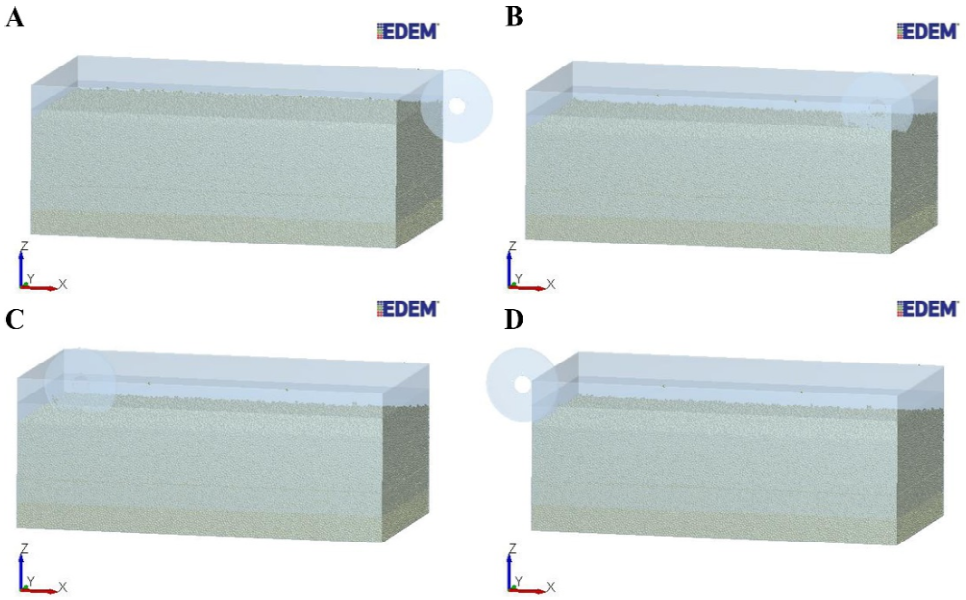

Fig. 4. Four stages of the interaction between the opener disc and the soil. A, the disc just contacting the soil; B, the disc fully immersed in the soil; C, the disc just leaving the soil; and D, the disc fully out of the soil.

Ten discs and soil interactions were simulated and analyzed. The results are shown in Table 3. BCDFOs showed a better furrow resistance performance than the CFDFO. The data were tested via range analysis according to extreme differences, and the factors were ordered based on importance (Ren, 2009a). The primary and secondary relationships of the test factors can be judged by the magnitude of the range R_j. R_j is the extreme difference of the j-column, which reflects the variation in the level of the j-column and the range of the test index. The larger the value is, the more important the factor is for the test results. The optimal level of test factors is determined by the average value of K_j, which represents the average value of the test index corresponding to the j-column factor under its level. The range analysis results of the above four factors were 29.77, 21.77, 68.13, and 83.33. With the furrow resistance as the evaluation index, θ was the key factor, followed by S_1, h_1 and D. The minimum resistance was found in DISC 3 (260.1 N) with θ=7.2°, S_1=6 mm, h_1=1 mm, D =14 mm and was approximately 45.43% less than the resistance of DISC 10. The resistance of DISC 2 and DISC 4 was 41.52% and 44.36% less than that of DISC 10, respectively.

Table 3 Furrow resistance of ten disc models simulated by DEM

Disc model	1	2	3	4	5	6	7	8	9	10
Resistance (N)	398.6	278.7	260.1	265.2	380.3	346.1	304.7	300.6	297.0	476.6

The disturbance and movement of soil were generated by the force exerted on the soil by the opener disc (Sun et al., 2018). The proper soil disturbance could improve the soil structure and control soil water loss (Rusinamhodzi, 2015). The structures of the disc affected the performance of the soil disturbance. The effects of different structures on soil disturbances in the forward and lateral directions of DISC 2, DISC 3, DISC 4 and DISC 10 are shown in Fig. 5. The soil swelling rate and soil disturbance coefficient are important indexes to evaluate the soil disturbance characteristics (Francetto et al., 2016). The soil swelling was the elevation area generated by the increase in voids between the soil. The soil swelling rate was equal to the ratio of the soil elevation area to the soil area before furrow. A lower soil swelling rate resulted in better soil backfill. The soil disturbance coefficient was equal to the ratio of the disturbed soil area to the soil area before furrowing. Less soil disturbance was required for conservation tillage; that is, the soil disturbance coefficient should be small, which would preserve the soil moisture and reduce the furrow resistance (Yao et al., 2007).

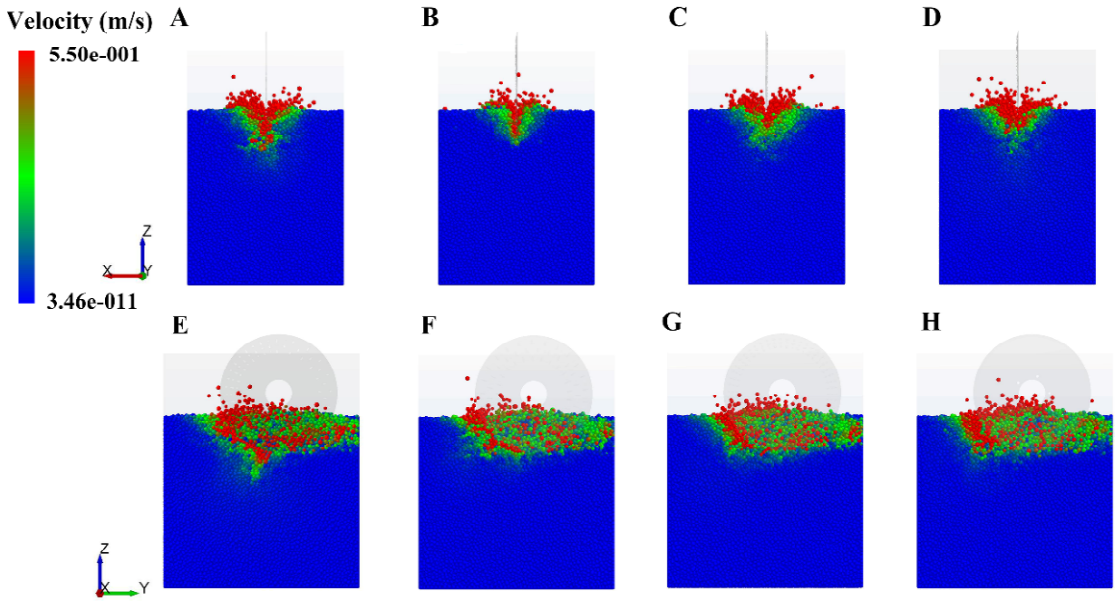

Fig. 5. Effect of different structures on soil disturbances in the forward and lateral direction. A, E: DISC 2, B, F: DISC 3, C, G: DISC 4, D, H: DISC 10.

The simulation results were loaded into Auto CAD software to calculate the soil swelling rate and soil disturbance coefficient, as shown in Fig. 6. The soil swelling rate of DISC 3 was the lowest, at 2.86%, followed by DISC 4, DISC 2 and DISC10 with swelling rates of 3.78%, 4.33% and 4.49%, respectively, which illustrated that the soil backfill of DISC 3 was best. The soil disturbance coefficient produced by DISC 3 was the lowest, at 3.91%, followed by DISC 4, DISC 2 and DISC10 with soil disturbance coefficients of 5.90%, 6.28% and 6.81%, respectively. This indicated that the size of biomimetic elements would affect the soil performance of cutting, shear and compaction, as described by Francetto (Francetto et al., 2016). Less soil disturbance could maintain greater soil moisture to facilitate seed growth. At the same time, it required less furrow resistance. Therefore, the furrow resistance of DISC 3 was the lowest, which was consistent with the simulation of furrow resistance.

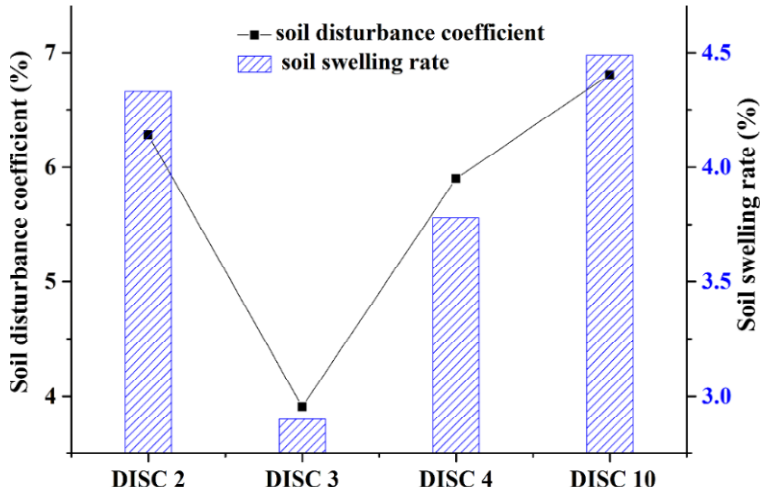

Fig. 6. Soil swelling rate and soil disturbance coefficient of DISC 2, DISC 3, DISC 4 and DISC10.

3.2 Analysis of the mechanical model

The whole opener process was divided into three steps: soil cutting, soil movement and slippage between the soil and opener disc.

3.2.1 The force produced by cutting the soil

Soil failure occurs during the movement process. According to the passive soil pressure model, the angle between the failure surface and horizontal plane was

$\left(\frac{\pi}{4}-\frac{\varphi}{2}\right)$, where φ was the soil internal friction angle, as shown in Fig. 7. The force analysis of the soil wedge showed that it was subjected to three forces: the soil shear resistance $d\tau$, the soil wedge gravity dW and the disc cutting force dP.

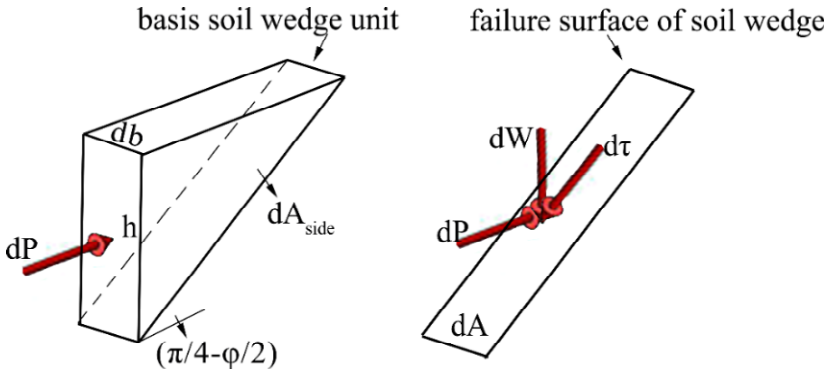

Fig. 7. Soil wedge model

According to the force balance equation, it is satisfied with *formula* 1 at the instant of failure as follows:

$$dP\cos\left(\frac{\pi}{4}-\frac{\varphi}{2}\right)-dW\sin\left(\frac{\pi}{4}-\frac{\varphi}{2}\right)=d\tau \quad (1)$$

Therefore, the soil wedge gravity dW satisfied *formula* 2 as follows:

$$dW=\rho_{soil}\times g\times dV_{soil}=\rho_{soil}\times g\times db\times A_{side}=\rho_{soil}\times g\times db\times\frac{h_{high}^{2}}{2\tan\left(\frac{\pi}{4}-\frac{\Phi}{2}\right)} \quad (2)$$

Data: ρ_{soil}—soil density; g—acceleration of gravity; dV_{soil}—volume of the basis soil wedge; A_{side}—lateral area of soil wedge; db—soil wedge width; h_{high}—soil wedge height.

Shear resistance $d\tau$ satisfied formula 3:

$$d\tau=c\times dA+dF\times\tan\varphi \quad (3)$$

Data: dF—normal positive pressure on the failure surface, $dF=dP\sin\left(\frac{\pi}{4}-\frac{\varphi}{2}\right)+dW\cos\left(\frac{\pi}{4}-\frac{\varphi}{2}\right)$; c—soil cohesion; A—contact area between the soil and disc.

Therefore, the disc cutting force dP was related to the soil cohesion, soil density, soil wedge width and soil wedge height.

3.2.2 The force produced by soil displacement

In the operational process, the opener disc advanced at a constant speed to cut the soil continuously, and the soil moved along the disc surface. Since soil movement

was a continuous process, the force acting on the disc could be calculated by the momentum impulse principle (Beer, 1965).

According to the momentum impulse principle, the equilibrium equation of the soil on the control body in the X and Y directions can be obtained as described below. In the X direction, the equilibrium equation is as follows:

$$-(\Delta m)v + F_x = -(\Delta m)v\cos\eta \quad (4)$$

In the Y direction, the equilibrium equation is as follows:

$$F_y = -(\Delta m)v\sin\eta \quad (5)$$

In the above equations, $\Delta m = \rho_{soil}V\Delta t = \rho_{soil}A_{forrow}v\Delta t = \rho_{soil}A\cos\alpha\cos\delta v\Delta t$; v—relative velocity of soil to the disc; η—the angle between displacement soil and horizontal plane; α—the front angle of opener disc; *??*—the disc angle of opener disc.

Combining the above formulas results in the following:

$$F_x = A\cos\alpha\cos\delta\rho_{soil}v^2(1-\cos\eta) \quad (6)$$

$$F_y = A\cos\alpha\cos\delta\rho_{soil}v^2\sin\eta \quad (7)$$

According to Newton's Third Law, action and reaction forces are equal in size and opposite in direction. Therefore, the force produced by soil displacement was related to the contact area between the soil and disc, the front and disc angle of the opener disc, the soil density, the relative velocity of the soil to the disc, and the angle between the displacement of soil and the horizontal plane.

3.2.3 Sliding resistance between soil and opener disc

The sliding resistance produced by the interaction of the opener disc and soil could be divided into two parts: the sliding resistance between the disc surface and soil during disc rotational and forward motion during ditching, and the friction force between the disc cutting edge and the soil. During the interaction process between the disc surface and the soil, in addition to the friction force, the adhesion force of the disc surface was also caused by the physical and chemical properties within the soil. The change in the adhesion force could affect the normal load of the contact interface. Therefore, the friction force of the disc surface was divided into two parts, friction

force and adhesion force, which were related to the absorption load caused by the water film, the attached area of the water film, the dynamic friction coefficient between the soil and the opener disc, and the quality of the opener disc (Gill and Vandenberg, 1983).

In summary, without considering the inherent characteristics of the soil, the opening resistance was related to the soil wedge width and height, contact area between the soil and disc, and the attached area of the water film, which all depended on the structures of the opener disc. When the biomimetic structural elements were applied to the opener disc, the disc structure could reduce the contact area between the soil and disc and the attached area of the water film, which reduced the effect of drag.

3.3 Soil bin test

According to the DEM simulation results, DISC 2, DISC 3 and DISC 4 had relatively low furrow resistance. Given possible calculation error, these three discs and CFDFO (DISC 10) were manufactured, as shown in Fig. 8. To investigate the tillage performance of furrow discs under different furrow speeds and soil moisture contents to verify the reliability of the simulation, soil bin tests of DISC 2, DISC 3, DISC 4 and DISC 10 were carried out.

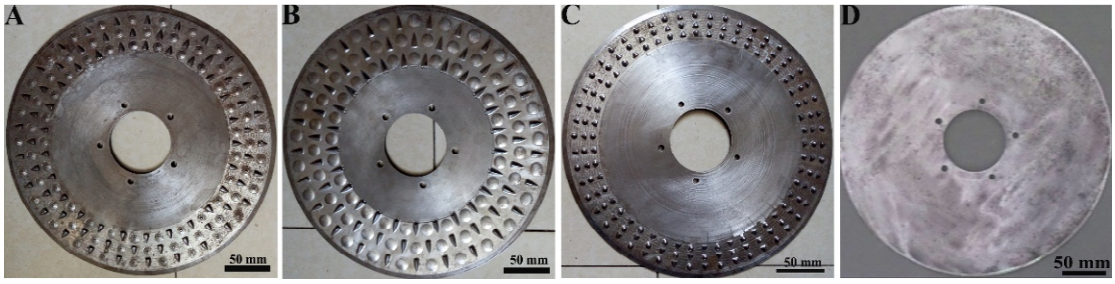

Fig.8. BCDFOs were manufactured according to DEM simulation. A: DISC 2, B: DISC 3, C: DISC 4, D: DISC 10 (CFDFO)

The test data were collected and arranged using a sensor built into the test vehicle and a data processing system. However, unstable signals were inevitable. Therefore, the force measuring system was calibrated and zero-set before formal test and pretesting. The data were collected and processed smoothly. In addition to erroneous individual data points (data with sudden increases or zero values), most of the remaining data points were relatively uniform and stable. Abnormal points were

removed from subsequent data processing. The furrow resistances of DISC 2, DISC 3, DISC 4 and DISC 10 under different conditions (soil moisture content = 18% and 22%; furrow speed = 0.6, 1 and 1.4 m/s) are shown in Fig. 9.

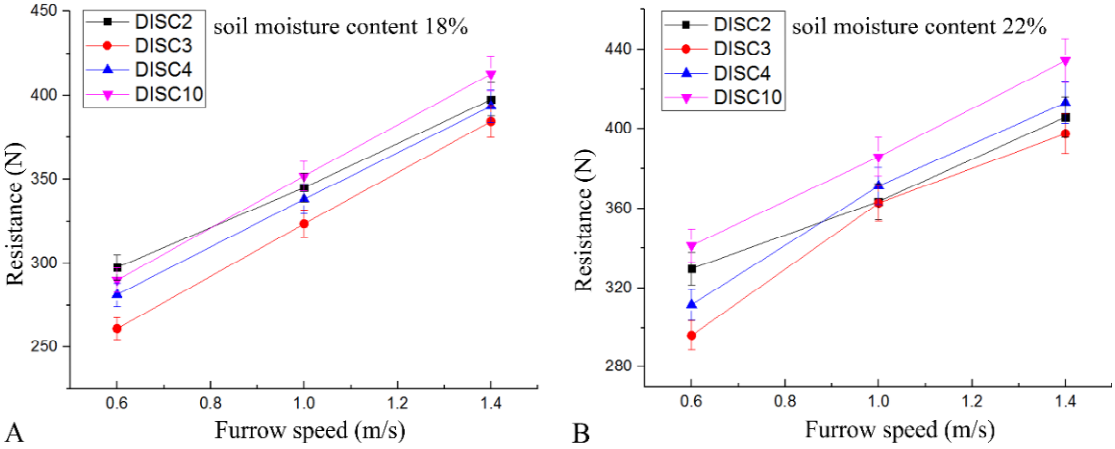

A B

Fig. 9. Soil bin resistance tests of DISC 2, DISC 3, DISC 4 and DISC 10 under different test conditions. A: soil moisture contents of 18% and B: soil moisture content of 22%.

Under the same test conditions, the furrow resistance of BCDFOs was obviously smaller than CFDFO. Under the condition of 18% soil moisture content, the furrow resistances of DISC 2, DISC 3, DISC 4 and DISC 10 increased by 15.96%, 23.89%, 20.19% and 21.37%, respectively, with the furrow speed increasing from 0.6 to 1.0 m/s and by 15.20%, 18.85%, 16.35% and 17.26%, respectively, and the furrow speed increasing from 1.0 to 1.4 m/s. However, under the condition of 22% soil moisture content, the furrow resistances of DISC 2, DISC 3, DISC 4 and DISC 10 increased by 10.24%, 22.42%, 19.13% and 13.07%, respectively, with the furrow speed increasing from 0.6 to 1.0 m/s and by 11.69%, 9.64%, 11.29% and 12.52%, respectively, with the furrow speed rising from 1.0 to 1.4 m/s. The resistance of all discs increased with increasing speed under the same soil moisture. This occurred because the higher speed of the disc would increase the accelerated soil mass and the rate of shear by the disc, which produced a higher resistance (Swick and Perumpral, 1988). With the increase in soil moisture content from 18% to 22% under the same speed, the furrow resistance of each disc increased. The soil condition affects the cutting, shear, compaction and flow performance of soil behavior (Collins and Fowler, 1996). This

occurred because the soil cohesion generated by water in the soil with higher gravimetric moisture content was increased. At the same time, the surface tension of the water film increased, which made the adhesion between the soil and disc greater, which led to decreasing the furrow quality and increasing the furrow resistance (Yao et al., 2007).

To compare the resistance reduction among the three BCDFOs, the drag reduction rate (DR) of BCDFOs was calculated as DR (%) = (furrow resistance of CFDFO –furrow resistance of BCDFO)/(furrow resistance of CFDFO) ×100%. The DRs of the three BCDFOs under different furrow speeds and moisture contents are shown in Table 4. The BCDFOs showed great drag reduction, of which the average DR of DISC 3 was 8.76% and that of DISC 2 was the lowest (3.14%). In summary, DISC 3 had the best drag reduction under different furrow speeds and soil moisture contents, which was consistent with the DEM simulation.

Table 4. DR of three BCDFOs under different test conditions

Soil moisture content (%)	Furrow speed (m/s)	DR (%)		
		DISC 2	DISC 3	DISC 4
18	0.6	-2.61	9.95	2.99
	1	1.97	8.08	3.92
	1.4	3.69	6.83	4.67
22	0.6	3.41	13.21	8.69
	1	5.83	6.04	3.81
	1.4	6.53	8.44	4.85
Average DR		3.14	8.76	4.82

4. Conclusions

The convex hull of the dung beetle pronotum and the back-ridge scales of the pangolin were used as biomimetic prototypes to improve and analyze the drag reduction of the disc furrow opener with non-smooth surfaces using an orthogonal experimental optimization design. The interactions of the discs and soil were simulated with DEM. Range analysis with resistance as the evaluation index indicated

that θ was the key factor, followed by S_1, h_1 and D. DISC 3 had the minimum resistance with θ=7.2°, S_1=6 mm, h_1=1 mm, D =14 mm.

The soil swelling rate and soil disturbance coefficient were important indexes to evaluate the soil disturbance characteristics. DISC 3 with a lowest soil swelling rate and soil disturbance coefficient required least furrow resistance, followed by DISC 4, DISC 2 and DISC10, which was consistent with the simulation of furrow resistance. Through the analysis of the mechanical model, the disc structure could reduce the contact area between the soil and disc and the attached area of the water film, which reduced the effect of drag.

Three BCDFOs (DISC 2-4) and one CFDFO were manufactured for soil bin tests under different conditions with the soil moisture contents of 18% and 22% and furrow speeds of 0.6, 1 and 1.4 m/s to investigate the relationships between surface structures and resistance. Under the same test conditions, the furrow resistance of BCDFOs was obviously smaller than that of the CFDFO. DISC 3 showed a maximum DR of 13.21% under a furrow speed of 0.6 m/s and a moisture content of 22%, and the maximum average DR of BCDFO was 8.76% under different furrow speeds and moisture contents. In summary, DISC 3 demonstrated the best drag reduction under different furrow speeds and soil moisture contents. These results will be helpful to design efficient disc furrow openers for resistance reduction with low soil disturbance.

Acknowledgements

This work was supported by National Key R&D Program of China (No. 2016YFE0112100), the China-EU H2020 FabSurfWAR Project (No. 644971), and the 111 project (No. B16020) of China, and the China Scholarship Council (CSC).

References

Ahmad, D., Amran, F., A. 2004. Energy prediction model for disk plow combined with a rotary blade in wet clay soil. Int. J. Eng. Technol. 1, 102-114.

Ahmadi, I., 2017. Effect of soil, machine, and working state parameters on the required draft force of a subsoiler using a theoretical draft-calculating model. Soil

Till. Res. 55, 389-400.

Asaf, Z., Rubinstein, D., Shmulevich, I., 2007. Determination of discrete element model parameters required for soil tillage. Soil Till. Res. 92, 227-242.

Barr, J., Fielke, J., 2016. Discrete element modelling of narrow tine openers to improve soil disturbance characteristics of no-till seeding systems. In: ASABE Annual International Meeting, Orlando, FL, United states.

Barr, J.B., Ucgul, M., Desbiolles, J.M., Fielke, J.M, 2018. Simulating the effect of rake angle on narrow opener performance with the discrete element method. Biosyst Eng. 171, 1-15.

Beer, F.P., 1965.Vector Mechanics for Engineers: Statics and Dynamics. McGraw-Hill Education, New York.

Budynas, R.G., Nisbett, K.J., 2012. Shigley's Mechanical Engineering Design. McGraw-Hill Education, New York.

Casao, R., de Araujo, A.G., Ralisch, R., 2000. Performance of MAGNUM 2850 seeder in nontillage in the basaltic soil of Parana, Brazil. Pesqui. Agropecu. Bras. 35, 523-532.

Chaudhary, M.A., 1988. A new multi crop inverted T seeder for upland crop establishment. AMA. 19, 37-42.

Chi, L., Kushwaha, R.L., 1990. A non-linear 3-D finite element analysis of soil failure with tillage tools. J. Terramechanics 27, 343-366.

Collins, B.A., Fowler, D.B., 1996. Effect of soil characteristics, seeding depth, operating speed, and opener design on draft force during direct seeding. Soil Till. Res.

39, 199-211.

Das, B.M., 2008. Advanced Soil Mechanics (3rd edition). Taylor and Francis, New York.

Deng J.Y., Liu X.M., Liu M.L., 1986. Experimental study on rat channel furrow opener. Grain Oil Process. Food Mach. 3, 3-10.

Francetto, T.R., Alonço, A.S., Brandelero, C., et al., 2016. Disturbance of Ultisol soil based on interactions between furrow openers and coulters for the no-tillage system. Span. J. Agric. Res. 14, 1-10.

Gill, W.R., Vandenberg, G.E., 1983.Tillage and Traction Soil Dynamics. China Agricultural Machinery Publish, Beijing.

Gou, W., Ma, R.C., Yang ,W.Y., et al., 2012. Design of opener on no-till wheat seeder. Trans. CSAE. 28, 21-25.

Jia, X., 2006. Unsmooth cuticles of soil animals and theoretical analysis of their hydrophobicity and anti-soil-adhesion mechanism. J. Colloid Interf. Sci. 295, 490-494.

Khan, A.S., Tabassum, M.A., Khan, J., 1990. Selection of seed-cum-fertilizer drill: technical considerations. AMA. 21, 35-39.

Mkomwa, S., Kaumbutho, P., Makungu, P., 2015. Farm Machinery for Conservation Agriculture. In: Conservation Agriculture, 109-131.

Ren, L.Q., 2009. Experimental Design and Optimization. Science Press.

Ren, L.Q., 2009. Progress in the bionic study on anti-adhesion and resistance reduction of terrain machines. Sci. China Ser. E 52, 273-284.

Ren, L.Q., Cong, Q., Tong, J., et al., 2001. Reducing adhesion of soil against loading shovel using bionic electro-osmosis method. J. Terramechanics 38, 211-219.

Rusinamhodzi, L., 2015. Crop rotations and residue management in conservation agriculture. In: Conservation Agriculture, Springer International Publishing.

Sakane, H., Maeyama, T., 1993. The mudless rotary tiller. Kubota Technical Report, 26, 27-31.

Salokhe, V.M., Gee-Clough, D., 1989. Application of enamel coating in agriculture. J. Terramechanics 26, 275-286.

Salokhe, V.M., Gee-Clough, D., 1988. Coating of cage wheel lugs to reduce soil adhesion. J. Agr. Eng. Res. 41, 201-210.

Salokhe, V.M., Gee-Clough, D., 1987. Formation of a boundary wedge on a single lug in wet clay soil. J. Agr. Eng. Res. 38, 113-125.

Spagnoli, G., Klitzsch, N., Fernandez-Steeger, T., et al., 2011. Application of electro-osmosis to reduce the adhesion of clay during mechanical tunnel driving. Environ. Eng. Geosci. 17, 417-426.

Sun, J.Y., Wang, Y.M., Ma, Y.H., et al., 2018. DEM simulation of bionic subsoilers (tillage depth>40 cm) with drag reduction and lower soil disturbance characteristics. Adv. Eng. Softw. 119, 30-37.

Swick, W.C., Perumpral, J.V., 1988. A model for predicting soil tool interaction. J. Terramechanics 25, 43-56.

Tong, J., Moayad, B.Z., Ma, Y.H., et al., 2009. Effects of biomimetic surface designs on furrow opener performance. J. Bionic Eng. 6, 280-289.

Tong, J., Ren, L.Q., Yan, J.L., et al., 1999. Adhesion and abrasion of several materials against soil. Int. Agr. Eng. J., 8, 1-22.

Ucgul, M., Fielke, J.M., Saunders, C., 2014. 3D DEM tillage simulation: Validation of a hysteretic spring (plastic) contact model for a sweep tool operating in a cohesionless soil. Soil Till. Res. 144, 220-227.

Wang, X.L., Ito, N., Kito, K., et al., 1998. Study on use of vibration to reduce soil adhesion. J. Terramechanics 35, 87-101.

Yao, Z.L., Gao, H.W., Wan,g X.Y., et al., 2007. Effect of three furrow openers for no-till wheat seeder on crop growth performance. Trans. CSAE 23, 117-121.

Zhang, Z.J., Jia, H.L., Sun, J.Y., 2016. Review of application of biomimetics for designing soil-engaging tillage implements in Northeast China. Int. J. Agr. Biol. Eng. 9, 12-21.

Zhao, S.H., Yang, Y.Q., Yan, Y.X., et al., 2013. Design of duck mouth type opener. J. Northeast Agr. U. 44, 113-117.

AMERICAN JOURNAL EXPERTS

EDITORIAL CERTIFICATE

This document certifies that the manuscript listed below was edited for proper English language, grammar, punctuation, spelling, and overall style by one or more of the highly qualified native English speaking editors at American Journal Experts.

Manuscript title:

DEM and soil bin study on a biomimetic disc furrow opener

Authors:

Yueming Wang, Weiliang Xue, Yunhai Ma, Jin Tong, Xianping Liu, Jiyu Sun

Date Issued:

November 10, 2018

Certificate Verification Key:

298D-A9A3-C7EC-D6DB-F8B1

This certificate may be verified at www.aje.com/certificate. This document certifies that the manuscript listed above was edited for proper English language, grammar, punctuation, spelling, and overall style by one or more of the highly qualified native English speaking editors at American Journal Experts. Neither the research content nor the authors' intentions were altered in any way during the editing process. Documents receiving this certification should be English-ready for publication; however, the author has the ability to accept or reject our suggestions and changes. To verify the final AJE edited version, please visit our verification page. If you have any questions or concerns about this edited document, please contact American Journal Experts at support@aje.com.